Published by :
http://www.ijert.org

International Journal of Engineering Research & Technology (IJERT)
ISSN: 2278-0181
Vol. 7 Issue 02, February-2018

Flow through Semi - Circular Obstructions in a Channel – Obstructions on Opposite Sides of the Channel

B. H. L. Gowda, B. K. Srinivas, V. Saifuddin , Shankar Bhandari, Anith Singh and A. Zaheer
Department of Mechanical Engineering,
BTL Institute of Technology, Bangalore-560099

***Abstract* -This paper presents flow visualization results for semi-circular constrictions in a two-dimensional channel. The constrictions are arranged on opposite sides of the channel. The relative size of the obstructions and the spacing between them is varied systematically. The results indicate that both these parameters have a significant influence on the flow field. The reattachment points, the wake structure change considerably with the variation of these parameters. The gap flow that occurs between the cylinders have a profound influence on the above mentioned features. The study brings out these effects.**

Keywords: Constrictions with semi-circular geometry, Channel, Obstructions on opposite sides, Interference effects.

INTRODUCTION

Obstructions occur on arterial walls mainly due to deposition of fatty material. Over a period of time these grow and occupy a substantial portion of the arteries. These are called stenotic obstructions and give rise to serious physiological conditions. The growth of the stenosis can be expected to be considerably influenced by the flow phenomena at various degrees of constrictions. There is a possibility of occurrences of another obstacle nearer to a previously formed one. This newly formed obstacle can occur on the same side or opposite side of the previous one. These obstacles can begin and grow simultaneously at the same rate or at different rates over a period of time or they can form one after another. It is essential to understand the flow past such obstructions and the resulting stresses on the lumen. To gain such understanding flow past simplified models of these obstructions with different geometries and varying sizes are made. The present study is one such investigation; semi-circular geometry is made use of and obstructions are considered on opposite sides of a channel wall.

Lakshmana Gowda [1] has considered flow through obstructions in a channel with different degrees of constrictions. He has considered rectangular, semi-circular, sinusoidal and plate geometries in a channel. The obstructions in all cases are located symmetrically at one location. It is reported that the flow field depends both on the degree of constriction and the Reynolds number. Depending on the two parameters mentioned, the flow downstream of the symmetrical constriction could be asymmetrical. However, no interference effects of more than one constriction is reported.

Griffith et. al.[2] have studied two-dimensional flow through a constricted channel. A semi-circular bump is located on one side of the channel and the extent of blockage is varied by adjusting the radius of the bump. The blockage is varied between 0.05 and 0.9 of the channel width and the upstream Reynolds number between 25 and 3000. The geometry presents a simplified blockage specified by a single parameter, serving as a starting point for investigations of other more complex blockage geometries. For blockage ratios in excess of 0.4, the variation of reattachment length with Reynolds number collapses to within approximately 15%, while at lower ratios the behavior differs. For the constrained two-dimensional flow, various phenomena are identified, such as multiple mini re-circulations contained within the main re-circulation bubble and vortex shedding at higher Reynolds numbers. The stability of the flow to three-dimensional perturbations is analyzed, revealing a transition to a three-dimensional state at a critical Reynolds number which decreases with higher blockage ratios. Separation lengths and the onset and structure of three-dimensional instability observed from the geometry of blockage ratio 0.5 resemble results taken from backward-facing step investigations. The question of the underlying mechanism behind the instability being either centrifugal or elliptic in nature and operating within the initial recirculation zone is analytically tested.

Sobey and Drazin [3] have investigated some instabilities and bifurcations of two-dimensional channel flows using analytical, numerical and experimental methods. They start by recapitulating some basic results in linear and nonlinear stability and drawing a connection with bifurcation theory. Then they examine Jeffery–Hamel flows and discover new results about the stability of such flows. Next they have considered two-dimensional indented channels and the resulting symmetric and asymmetric flows. It is demonstrated that the unique symmetric flow which exists at small Reynolds number is not stable at larger Reynolds number, there being a pitchfork bifurcation so that two stable asymmetric steady flows occur. At larger Reynolds number it is found as many as eight asymmetric stable steady solutions, and the existence of another seven unstable solutions inferred. When the Reynolds number is sufficiently large they find time-periodic solutions and deduce the existence of a Hopf bifurcation. These results show a rich and unexpected structure to solutions of the Navier–Stokes equations at Reynolds numbers of less than a few hundred.

(This work is licensed under a Creative Commons Attribution 4.0 International License.)

International Journal of Engineering Research & Technology (IJERT)
ISSN: 2278-0181
Vol. 7 Issue 02, February-2018

Mandal and Chakrabarthi [4] have carried out a numerical study for rectangular stenosis with different stenosis length and for degree of constriction 50%. Wall pressure, streamline contour, axial velocity profile, wall shear stress have been studied and their psychological aspect have been discussed. It was reviled that the pressure drop and wall shear stresses are dependent upon the stenosis length. Axial velocity profile and reattachment length are relatively independent of stenosis length. During initiation of stenosis length, the appreciable increase in the peak wall shear is noted, this magnitude of weak wall shear stress is observed to be decreasing with the progression of stenosis length. There is no change in size of recirculation zone, axial velocity profile and low shear stress with stenosis length. Therefore, the chance of tearing action and collapse of endothelium wall increases with the progression of stenosis length, as the wall pressure is thought to be one of the prime causes of this phenomenon. Since recirculation zone is not depending on the stenosis length, therefore it can be stated that during initiation of the stenosis length, maximum possibility of lipid deposition on the wall may take place, but the phenomenon may not take place with further increase in stenosis length. The maximum cell turnover point on the arterial wall due to reattachment point moves downstream with stenosis length. Wall damage and decrease with the progression of stenosis length.

There appears to be very little information on the interference effects of the obstructions when more than one is present on the flow field. In this study, flow past semi-circular obstructions arranged on opposite sides of a channel with varying relative sizes is investigated. The geometry is similar to that used by Griffith et al [2] but with two obstructions on the opposite sides of the channel. Flow visualization is made use of for the investigation. The configuration considered is shown in Fig.1. The length of the channel is L and the width W. The radius of the upstream semi-circular block is r and the radius of the interfering block is r_i. The center to center distance between the obstructions is s.

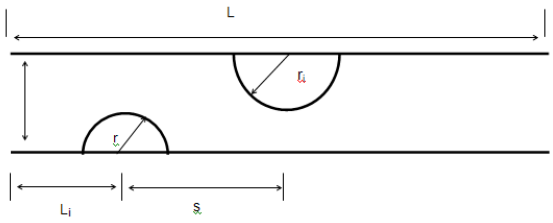

Fig. 1 Configuration considered

EXPERIMENTAL ARRANGEMENT

Experiments have been conducted using Flow Visualization Facility which is available at the fluid mechanics laboratory, Department of Mechanical Engineering, B.T.L. Institute of Technology. This facility consists of a F.R.P tank with 2.5 m length and breadth of 1.5 m (Fig. 2) and a set of aluminum discs, separated by a small distance are located at one end of the tank. The discs are connected to a three phase induction motor with cooling arrangement through a set of bevel gears and the flow created from the rotation of the discs is guided into the test section by two guide blocks made of FRP. The width of this test section is 350mm. By controlling the speed of the motor, the speed in test section could be varied continuously up to 0.2 m/s. At higher speeds the water becomes wavy and hence for the experiments a suitable speed is chosen where such waves do not occur. Fine aluminum powder is used as a tracer medium. Single-Lens Reflex (SLR) camera is be used to photograph the flow field. The camera is placed at a suitable height above the channel containing baffle plates. Two Halogen 500 watts lamps are used to obtain proper lighting.

The semi-circular models are made out of 2 mm thick mild steel plates and fixed to the sides of a channel 50 mm wide (W). The radii of the upstream obstruction (r) and the downstream interfering obstacle (r_i) used are 20 mm, 25 mm, 37.5 mm and 45 mm. The degree of constriction, D, is defined as r/W and the relative constriction ratio is defined as r/r_i. The spacing ratio L_s is defined as s/W where s is the distance between the centers of the two obstructions (Fig.1). The Reynolds number is defined as 2UW/ν where U is mean velocity in the channel and ν is the kinematic viscosity. All the cases considered here have same free stream velocity U = 0.073m/sec and Reynolds number is kept constant as 9125. The experiment is carried out by keeping the upstream obstacle of constant radius to get r/W = 0.4, 0.5, 0.75 and 0.9. For each r/W the radius of the downstream obstacle is varied to get D = 0.4, 0.5, 0.75 and 0.9. For each of this combination, interference length ratio is varied as L_s= 2, 2.5, 3, 4 and 5 and results obtained.

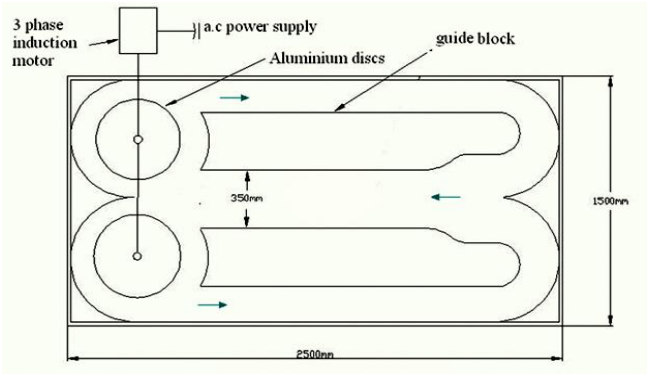

Fig. 2: Experimental arrangement

RESULTS

The results have been obtained for r/w = 0.4, 0.5, 0.75 and 0.9 and for each r/w, r_i/w = 0.4, 0.5, 0.75 and 0.9. However, results with r_i/w = 0.4 are not presented to restrict the number of pages. To obtain a better prospective of the results with interference, results for the case without interference (i.e., single semi-circular cylinder with different r/w values) is presented first in Fig.3.

From Fig.3, it is seen that the area of the flow decreases as the obstacle is introduced with increasing value of D (degree of constriction) of the obstacles. Flow separation takes place when it passes through the gap between the obstacle and the channel wall due to the adverse pressure gradient occurring on the downstream side of the obstacle. Due to this separation there is a formation of re-circulation zone and an ellip-

(This work is licensed under a Creative Commons Attribution 4.0 International License.)

International Journal of Engineering Research & Technology (IJERT)
ISSN: 2278-0181
Vol. 7 Issue 02, February-2018

tical vortex formation is observed in the recirculation zone. As D is increased, vortex formation becomes prominent and vortex shedding is observed due to which recirculation zone is increased. When D is 0.75 a wall jet flow is observed, a stagnant zone is found in behind the obstacle. The reattachment length is observed to increase with increase in the degree of constriction.

When an obstacle with $r_i/W = 0.5$ (with $r/W = 0.4$) is introduced on the opposite side of the channel wall at the interference length ratio s/W=2 as shown in Fig.4b, the downstream obstacle interferes with the flow field and the recirculation zone immediately behind the upstream obstacle. This is due to the gap flow between the two which is strongly biased downwards. As a result, the recirculation region behind the front obstacle is shortened and there is a large recirculation zone behind the opposite downstream obstacle with a series of vortical patterns. At s/W = 2.5 (Fig.4c) the recirculation zone behind the front obstacle lengthens and that behind the opposite downstream obstacle slightly reduces. This process of lengthening behind the front and shortening behind the rear obstacles continue at s/W = 3 (Fig.4d). With further increase in s/W, at 4 and 5 (Figs.4e and f), there is very little change in the flow field.

For $r_i/W = 0.75$ (Fig.5), at s/W = 2 (Fig.5b), due to the increase in the radius of the obstacle, the downstream obstacle causes the flow to turn steeply and a jet like flow occurs at the bottom. The separation zone behind the front obstacle is very small and the wake behind the rear cylinder extends for a long distance downstream. At s/W = 2.5 (Fig.5c), the steepness in the biased flow reduces with changes in the wake patterns behind both the obstacles. The jet like flow below the rear cylinder seems to become stronger and persists for a long distance downstream. At higher value of s/W (3, 4 and 5, Figs.5d, e and f)the bias in the gap flow between the cylinders continuously decreases. Wakes behind both the cylinders tend to decrease with reattachment points forming.

When the height of the interfering obstruction r_i/W increases to 0.9 (Fig.6), at s/W = 2 (Fig.6b), the separation region behind the front cylinder almost disappears. A strong jet like flow streams from the gap between the channel wall and the downstream obstacle. A large near stagnant flow is created behind the top obstacle. As the spacing between the obstacles increase, the recirculation region behind the front obstacle reappears and gradually increase in size (Figs. 6c to f). However, the changes in the wake behind the rear obstacle are marginal due to the jet issuing from the gap between the obstacle and the channel wall.

The results for the case with $r/W = 0.5$ and $r_i/W = 0.5$ at various values of s/W are shown in Fig.7b to 7f. As s/W varies from 2 and 3 (Figs.7b, c and d) the bias in the gap flow decreases. The wake behind the front obstacle gradually increases, the length of the separation zone behind the downstream obstacle consisting of a series of weak vortical patterns. At s/W = 4 and 5 (Figs. 7e and f) the bias in the vicinity of the upstream body has almost disappeared with similar near wakes. The flow in front and behind the rear obstacle change very little for these two spacings.

When $r_i/W = 0.75$ (Fig.8), at s/W = 2, there is a well defined recirculation region behind the front obstacle. The strong downward biased flow attaches on part of the downstream obstacle and then separates. Because of this a streaming flow occurs at the bottom wall and a large wake with weak vortical patterns are formed behind the downstream obstacle. At s/W = 2.5, the recirculation region behind the front body lengthens and that behind the rear, shortens. The attachment length on the rear body reduces due to the decreased bias of the flow between the cylinders. As s/W changes to 3 and 4, the recirculation length behind the front body increases. Behind the rear body also, the wake length tends to increase with s/W. There is very little change in the flow patterns between s/W = 4 and 5.

Figure 9 shows the results for $r/W = 0.5$ and $r_i/W = 0.9$ for different spacing. The result at Fig.9a is for the single obstacle. At s/W = 2, there is a stationery vortex behind the front obstacle. The recirculating region behind the front body increases with s/W up to 4. The flow separation region in front of the rear obstacle shows a changing pattern with s/W. As s/W increases the extent of this separation region increases due to the change in the bias of the gap flow between the two obstacles. It is interesting to observe local separation zones upstream of the rear obstacle at s/W = 4 and 5 caused due to the changed path of the biased flow between the obstacles. Further, it is seen that the jet like flow between the bottom surface of the rear body and the channel wall persists for long distances downstream. This has a significant effect on the wake structure behind the rear obstacle. A near stagnant wake is formed whose length is slightly altered with s/W.

For $r/W = 0.75$ and $r_i/W = 0.5$ results are shown in Fig.10, The flow pattern for the single obstacle is shown in Fig.10a. With the presence of the interfering obstacle on the opposite side (Figs.10b to f) there is a marked change in the flow . The gap flow created changes the recirculation region behind the front body. It decreases (s/W =2) and then increases with s/W. However there is very little change between s/W = 4 and 5. The gap flow attachment on the downstream obstacle and then the detachment causes changes in the wake behind the downstream obstacle whose length varies with s/W (Fig.10b to f). Also a separation region occurs in front of the rear body whose length slightly varies with s/W.

At $r_i/W = 0.75$ (Fig.11), the gap flow pattern is much different from that seen for $r_i/W = 0.5$. At s/W = 2, the flow which separates from the top of the front obstacle, attaches on to the rear obstacle and then moves down. This tendency is seen to persist at all other values of s/W. Because of this the recirculation region behind the front obstacle changes both in shape and length. The strong jet like flow emanating from the gap near the wall below the downstream obstacle proceeds along the wall for considerable downstream distance. The wake behind the rear body consists of nearly a dead water region with weak vortical flows. All these features can have significant effect on the shear force distribution on the walls of the channel.

(This work is licensed under a Creative Commons Attribution 4.0 International License.)

International Journal of Engineering Research & Technology (IJERT)
ISSN: 2278-0181
Vol. 7 Issue 02, February-2018

The results for r/W = 0.75 and r_i/W = 0.9 are shown in Fig.12. In Fig.12a for the single obstacle, a long recirculation region with a number weak vortical patterns is seen. With the interfering obstacle on the opposite side there is a dramatic effect on the flow. The resulting gap flow flows between the obstacles and forms a wall jet flow downstream. Just behind the rear obstacle there is a long dead water region with weak vortical pattern. There is a small separated region behind the front obstacle. As the gap between the two obstacles increase (s/W = 2.5, 3, 4 and 5; Figs 12 b to f)the wake behind the front obstacle increases. The gap flow attachment point on the front face of the rear obstacle changes (seem to have a unsteady character). The wall jet flow emanating from the narrow bottom gap below the rear obstacle shows a slight upward bend. This influences the near wake formation and its length behind the rear obstacle. The length is seen to decrease with increase in s/W = 3 to 5 (Figs.12d tof). The separation zone in front of the rear body appears to remain same at all values of s/W.

The results for r/W = 0.9 and r_i/W = 0.5, 0.75 and 0.9 at various spacing are shown in Figs. 13, 14 and 15 respectively. For the single body (Fig.13a), the flow from the gap at the top issues in the form of a jet and a large wake behind the body with weak vortical flow is formed. With the obstruction (Fig.13b), the gap flow bends and attached flow occurs on the upstream body. A strong flow is seen on the front face of the downstream obstacle and then separating flow. The separating flow attaches downstream on the channel wall. With increase in s/W (2.5, 3 and 4; Figs.13c, d and e) the wake length behind the front body increases due to the ensuing gap flow and its attachment on to the downstream body. The separation zone in front of the rear body increases with s/W and also the wake behind the body changes. Between s/W = 4 and 5 (Figs.13e and f) there is very little change.

When r_i/W = 0.75, at s/W = 2 (Fig.14b), the wake behind the front body almost disappears due to the strong gap flow. Further the jet like flow issuing from the narrow gap below the downstream body extends for a long distance downstream and a long recirculation region with weak vortices are seen. With increasing s/W (Figs.14c to f), the wake behind the front body and the separation zone in front of the rear body increases. The strong jet issuing from the gap below the rear obstacle causes a large near dead water region behind the rear obstacle. For r_i/W = 0.9, at various values of s/W (Figs.15 b to f), the above description holds good except the stronger gap flow jet emanating between the bottom of the downstream obstacle and the channel wall. As this gap flow appears to be stronger than for r_i/W = 0.75 Fig. 14), longer regions of nearly stationery fluid with a complex pattern of vortical patterns are seen.

CONCLUDING REMARKS

Flow visualization results when two obstructions with semicircular geometry have been presented. The obstructions are placed on opposite sides of the channel walls. The effects of the change in the relative size of the obstructions are investigated.

The results indicate that both the relative size and spacing have a profound effect on the flow field. The most important effect appears to be the formation of the gap flow with the presence of the downstream obstacle on the opposite side of the channel wall. In general the bias in this gap flow increases with the increase in the relative size of the obstacle for smaller values of s/W. The other factors which have considerable effect on the flow field are the gap flow from the front body and the channel wall and the corresponding gap flow between the rear body and the channel wall. Especially the latter influences the wake behind the rear obstacle considerably. Another aspect of interest is the wake formed in front of the rear obstacle whose length changes with the spacing.

The changes in the flow field seen with interference effect has considerable influence on the stresses created on the channel walls. Such situations occur around obstructions/stenoses created in an artery. The present study helps to understand the flow field changes that could occur in real situations.

ACKNOWLEDGEMENTS

The authors express their sincere thanks to the management of BTL IT for their support and encouragement.

REFERENCES

[1] B. H. Lakshmana Gowda. A Kaleidoscopic View of Fluid Flow Phenomena, Published by Wiley Eastern Limited (1992).
[2] M. D. Griffith, M. C. Thompson, T. Leweke, K. Hourigan and W. P. Anderson. Wake Behaviour and Instability of Flow through a Partially Blocked Channel. J. Fluid Mech. (2007), vol. 582, pp. 319–340.
[3] Ian J. Sobey and Philip G. Drazin, Bifurcations of two-dimensional channel flows, J. of Fluid Mmechanics, vol. 171, pp. 263-387.
[4] D. K. Mandal and S. Chakrabarti, Effect of Stenosis Length on Flow Characteristics Across Rectangular Stenotic Models, International J. of Fluid Mechanics, vol. 5(1) (2013); pp. 29-39.

NOMENCLATURE

L = length of the channel

W = Width of the channel

s = distance between the centre of the obstacles

r = radius of upstream obstacle

r_i = radius of downstream obstacle

Degree of constriction D = r/W

Relative spacing ratio: s/W

(This work is licensed under a Creative Commons Attribution 4.0 International License.)

International Journal of Engineering Research & Technology (IJERT)
ISSN: 2278-0181
Vol. 7 Issue 02, February-2018

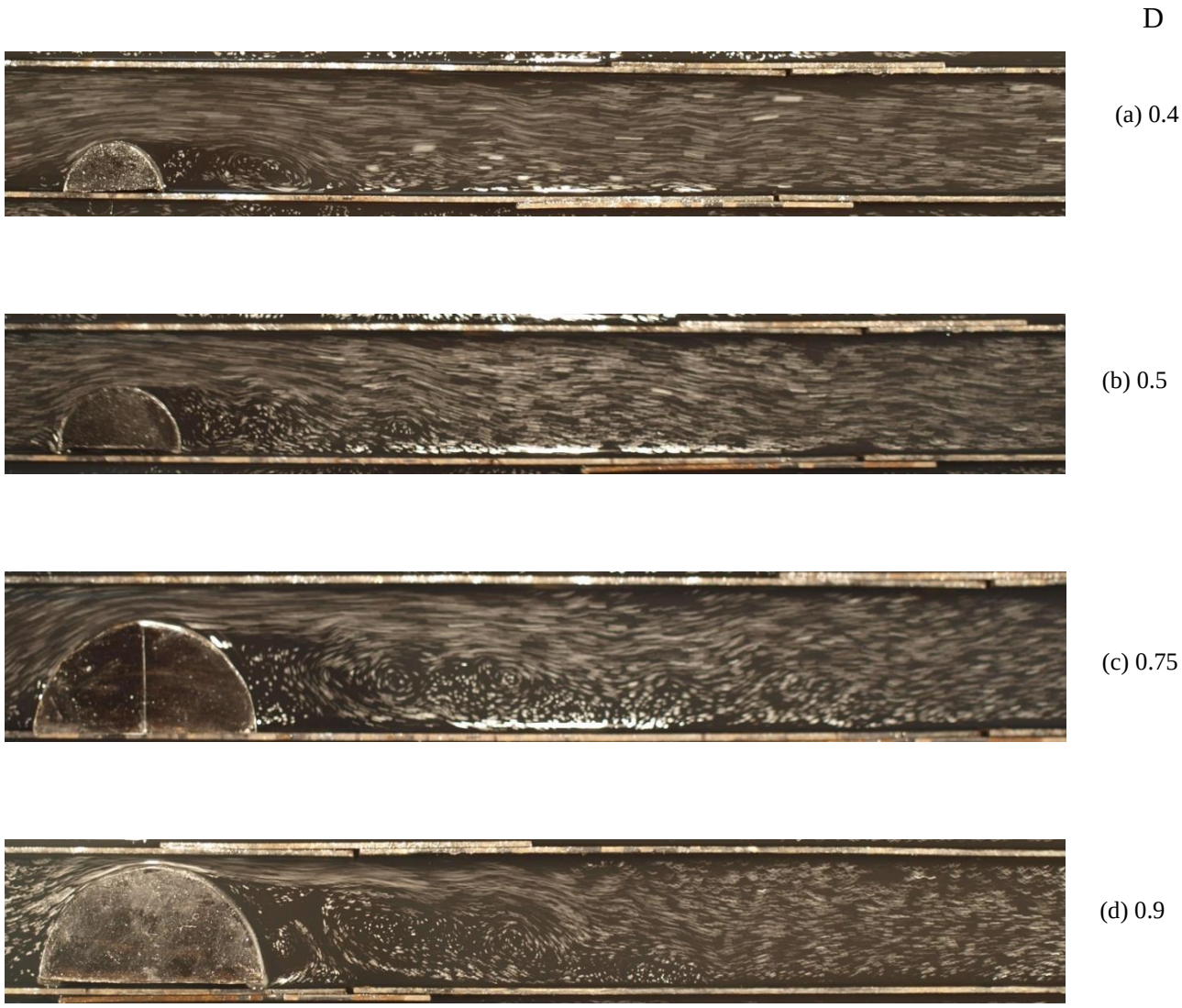

Fig.3 Flow field for single obstacle, for various Degree of Constriction (D)

(This work is licensed under a Creative Commons Attribution 4.0 International License.)

International Journal of Engineering Research & Technology (IJERT)
ISSN: 2278-0181
Vol. 7 Issue 02, February-2018

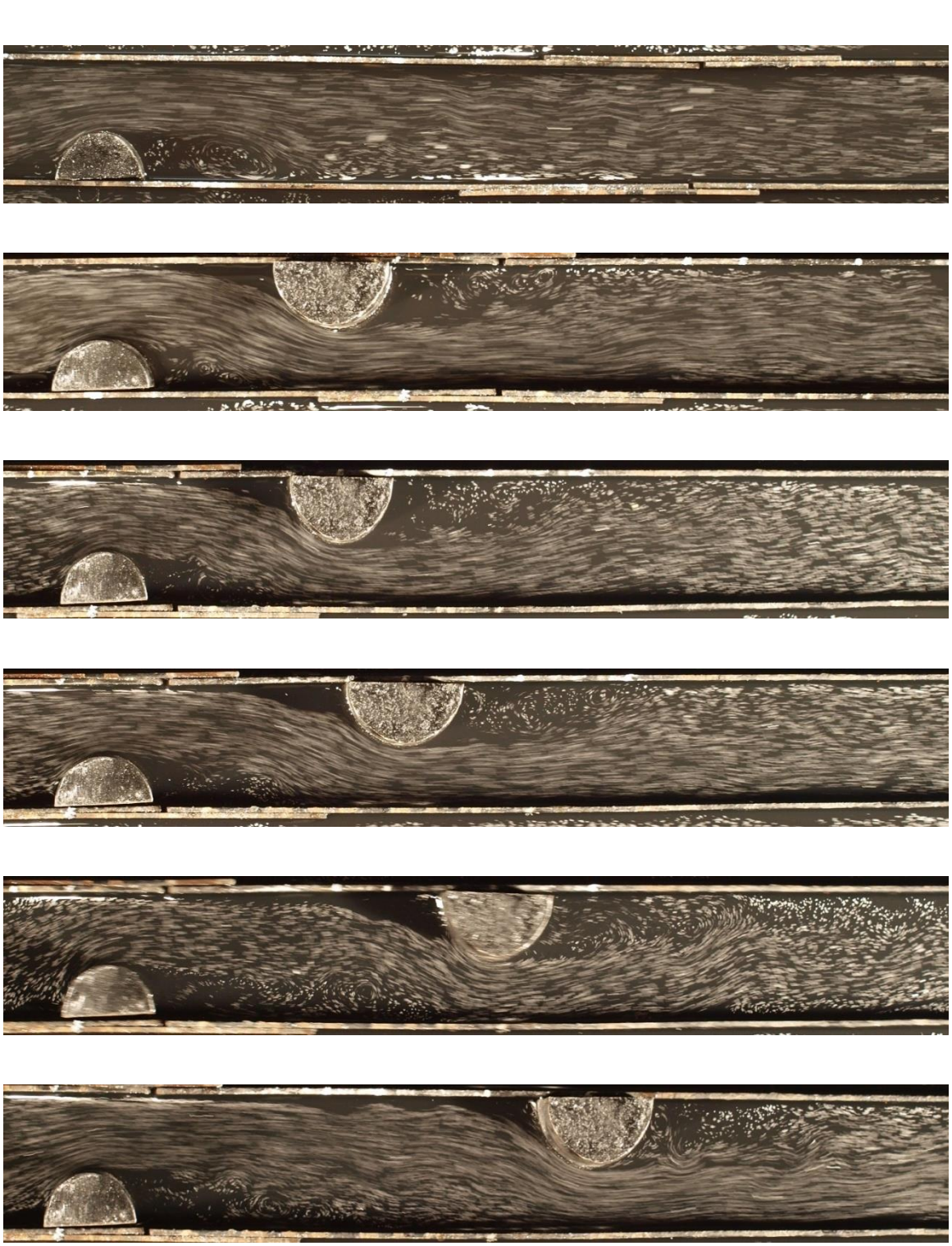

Fig.4 Flow pattern for r/W=0.4, r_i/W=0.5, for various s/W ratio.

(This work is licensed under a Creative Commons Attribution 4.0 International License.)

International Journal of Engineering Research & Technology (IJERT)
ISSN: 2278-0181
Vol. 7 Issue 02, February-2018

s/W

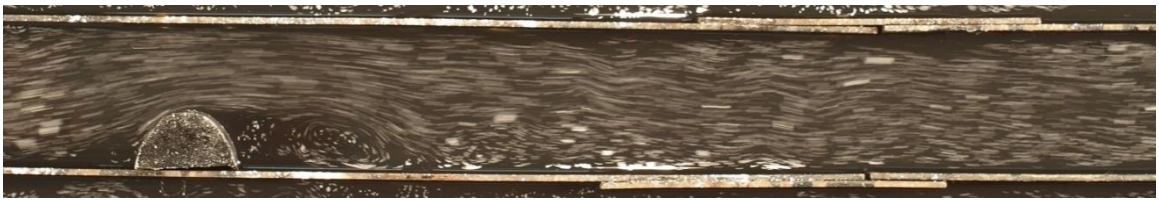

(a)

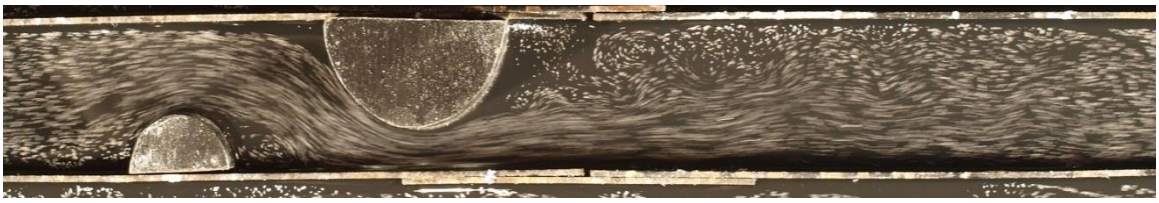

(b)

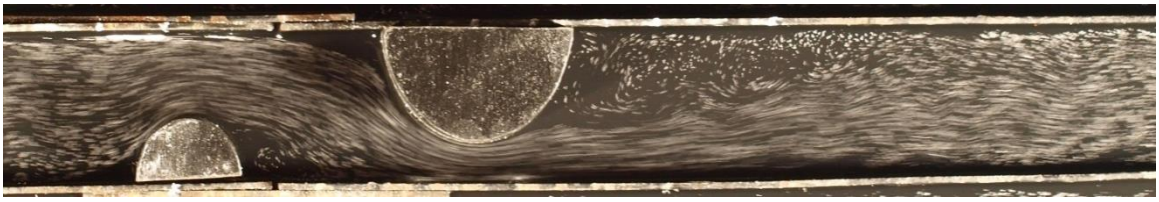

(c) 2.5

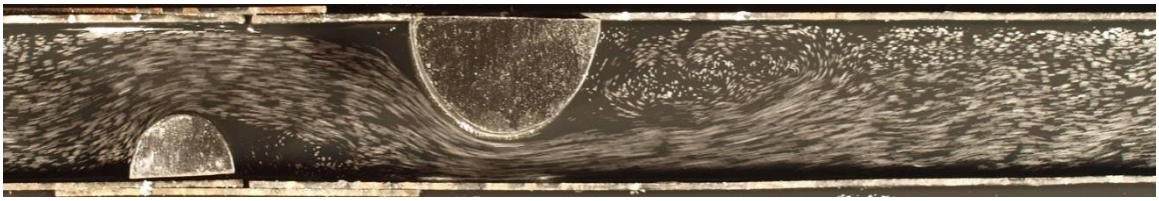

(d) 3

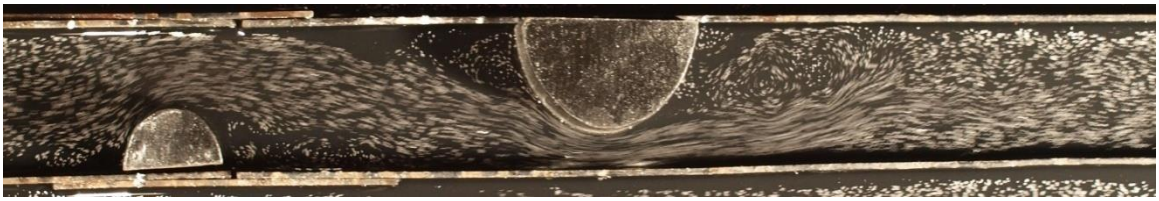

(e) 4

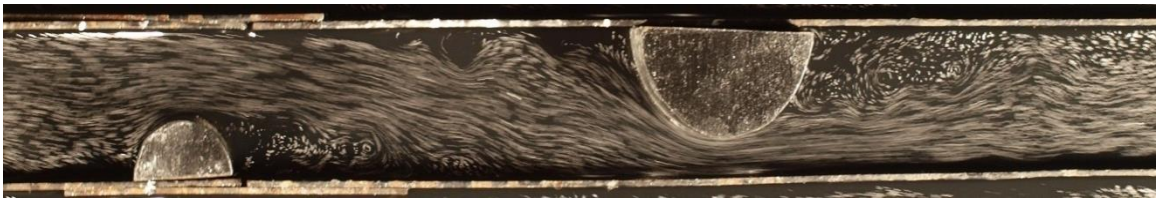

(f) 5

Fig.5 Flow pattern for r/W=0.4, r_i/W=0.75, for various s/W ratio.

(This work is licensed under a Creative Commons Attribution 4.0 International License.)

International Journal of Engineering Research & Technology (IJERT)
ISSN: 2278-0181
Vol. 7 Issue 02, February-2018

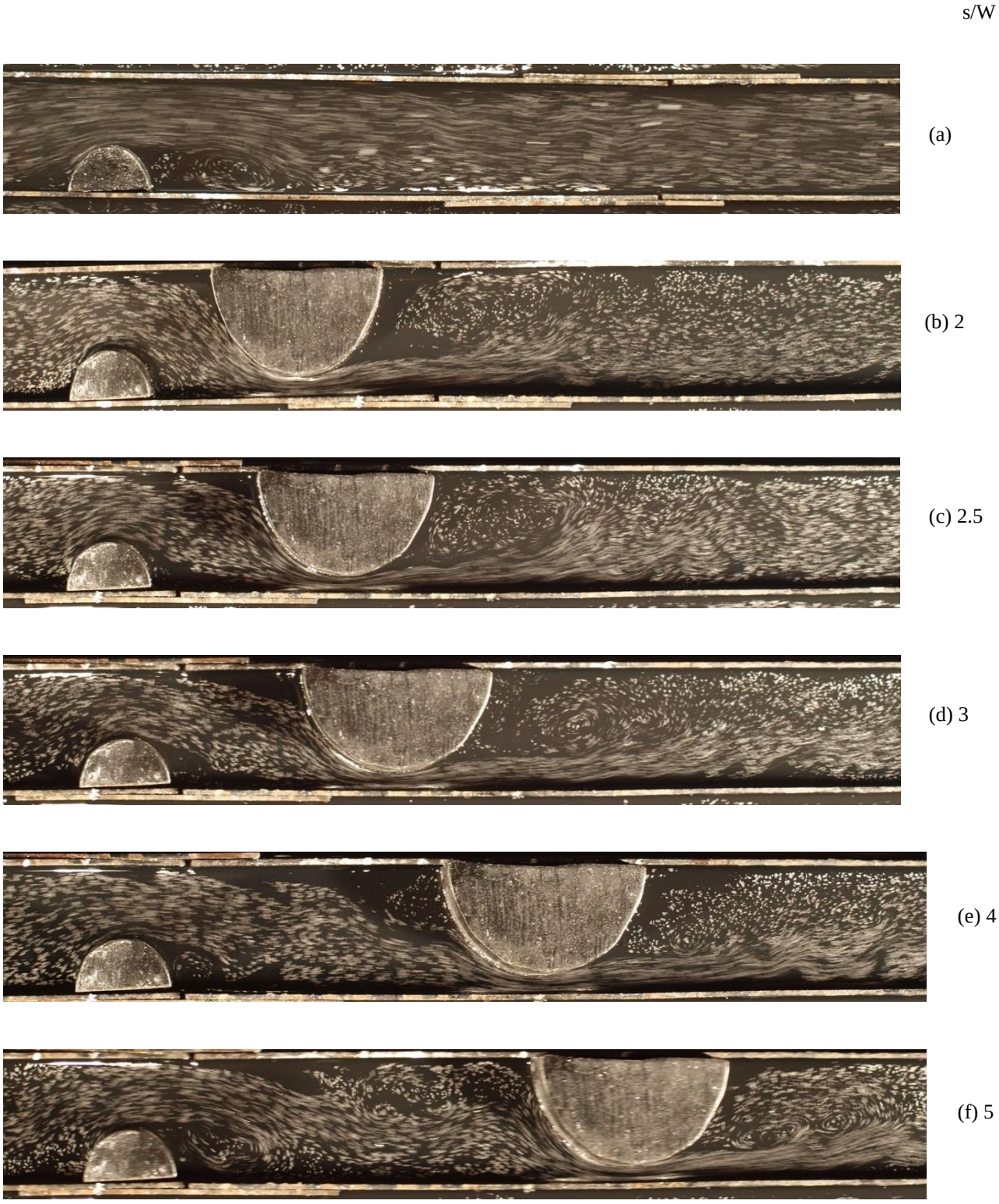

Fig.6 Flow pattern for r/W=0.4, r_i/W=0.9, for various s/W ratio.

(This work is licensed under a Creative Commons Attribution 4.0 International License.)

International Journal of Engineering Research & Technology (IJERT)
ISSN: 2278-0181
Vol. 7 Issue 02, February-2018

s/W

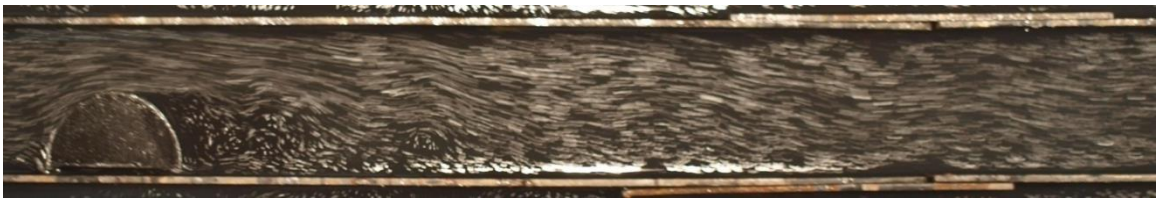

(a)

(b) 2

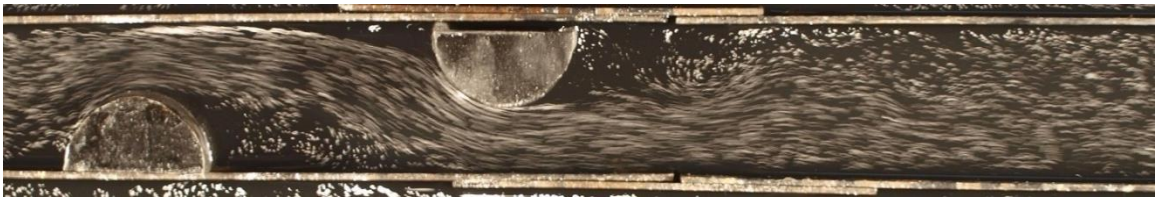

(c) 2.5

(d) 3

(e) 4

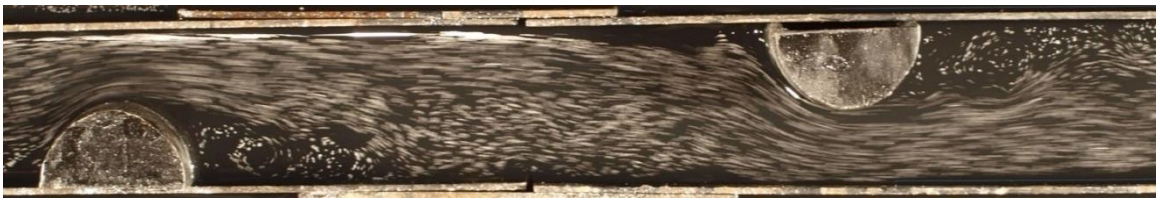

(f) 4

Fig.7 Flow pattern for r/W=0.5, r_i/W=0.5, for various s/W ratio.

(This work is licensed under a Creative Commons Attribution 4.0 International License.)

International Journal of Engineering Research & Technology (IJERT)
ISSN: 2278-0181
Vol. 7 Issue 02, February-2018

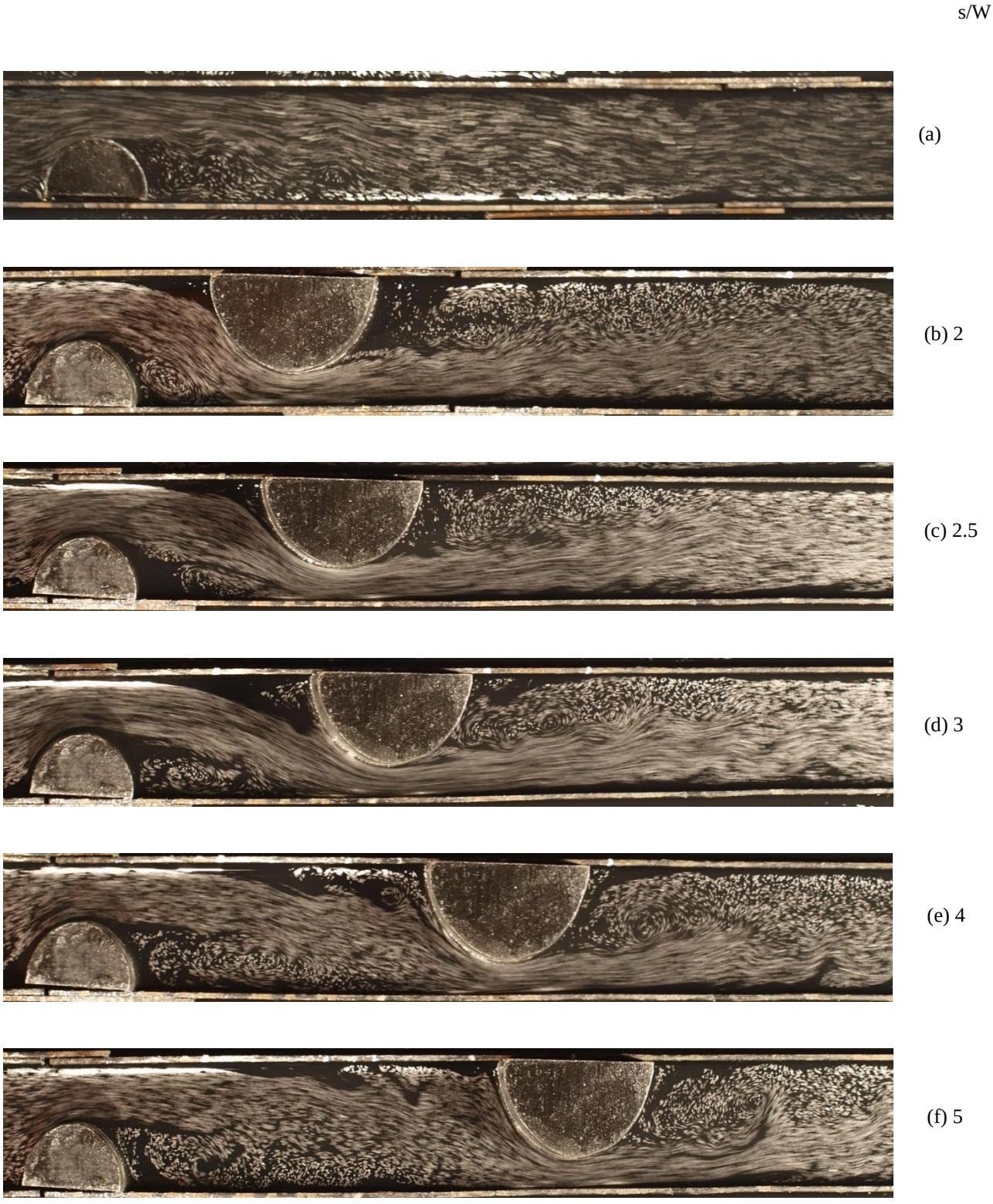

Fig.8 Flow pattern for r/W=0.5, r_i/W=0.75, for various s/W ratio.

(This work is licensed under a Creative Commons Attribution 4.0 International License.)

International Journal of Engineering Research & Technology (IJERT)
ISSN: 2278-0181
Vol. 7 Issue 02, February-2018

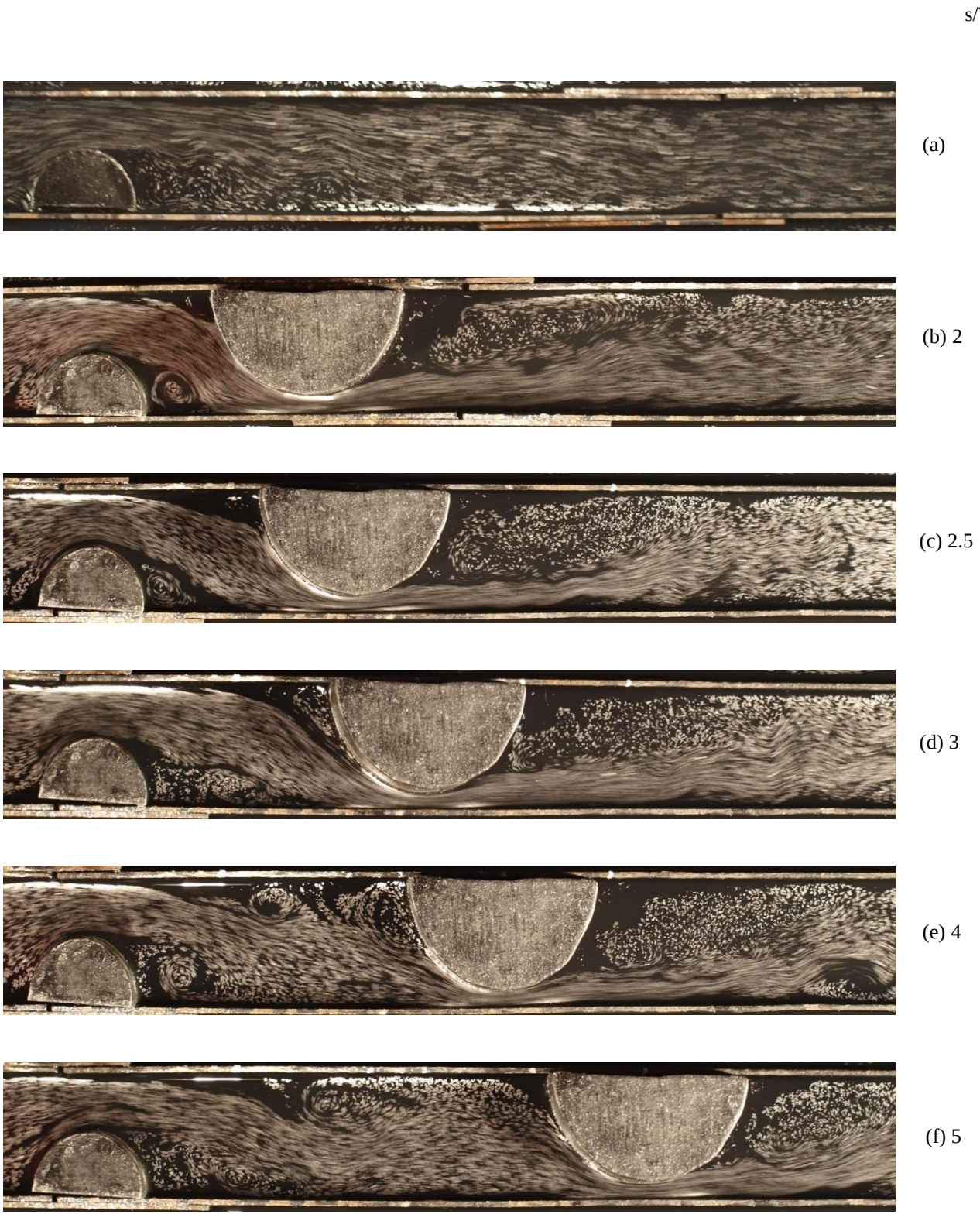

Fig.9 Flow pattern for r/W=0.5, r_i/W=0.9, for various s/W ratio.

(This work is licensed under a Creative Commons Attribution 4.0 International License.)

International Journal of Engineering Research & Technology (IJERT)
ISSN: 2278-0181
Vol. 7 Issue 02, February-2018

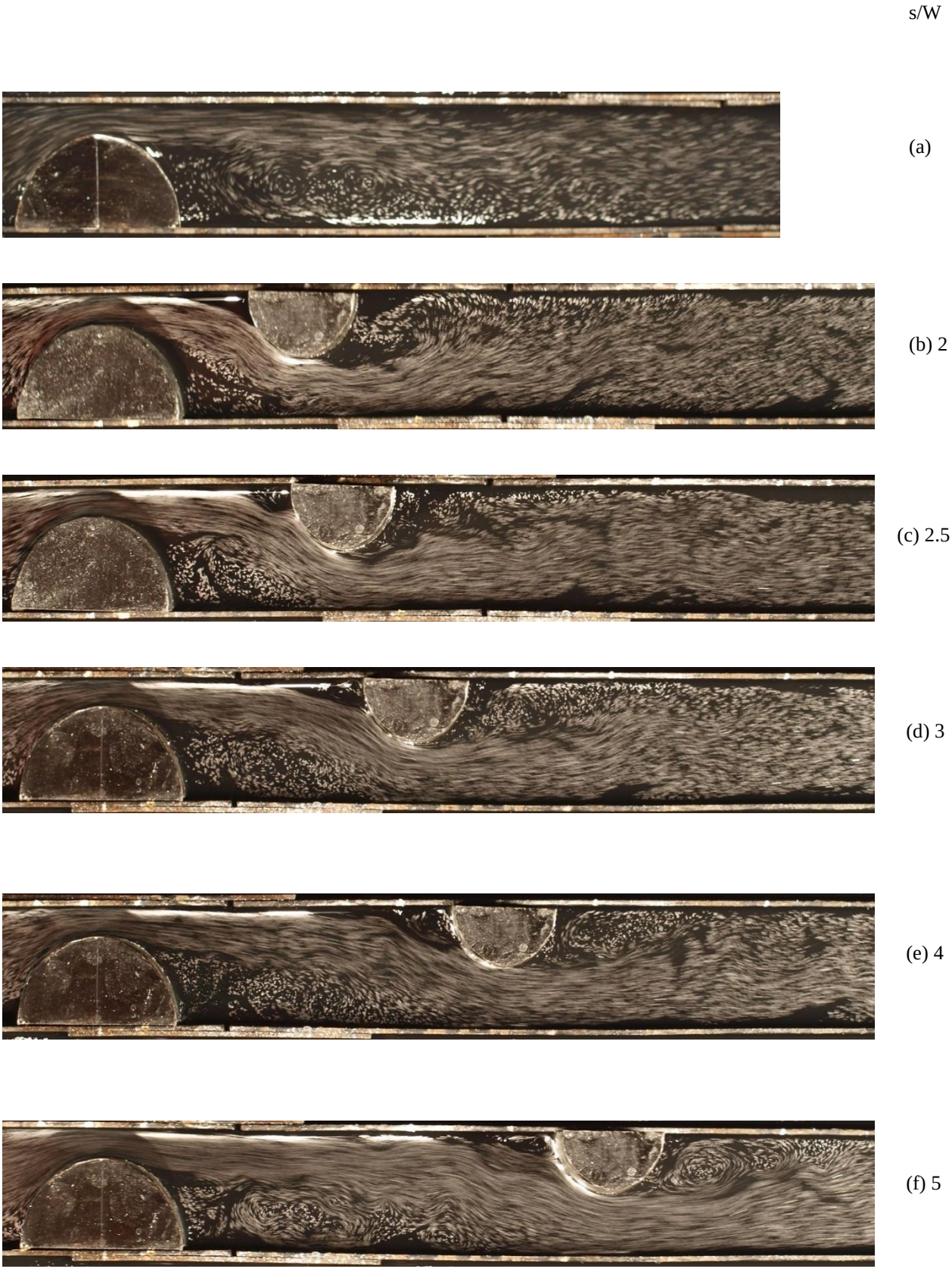

Fig.10 Flow pattern for r/W=0.75, r_i/W=0.5, for various s/W ratio.

(This work is licensed under a Creative Commons Attribution 4.0 International License.)

International Journal of Engineering Research & Technology (IJERT)
ISSN: 2278-0181
Vol. 7 Issue 02, February-2018

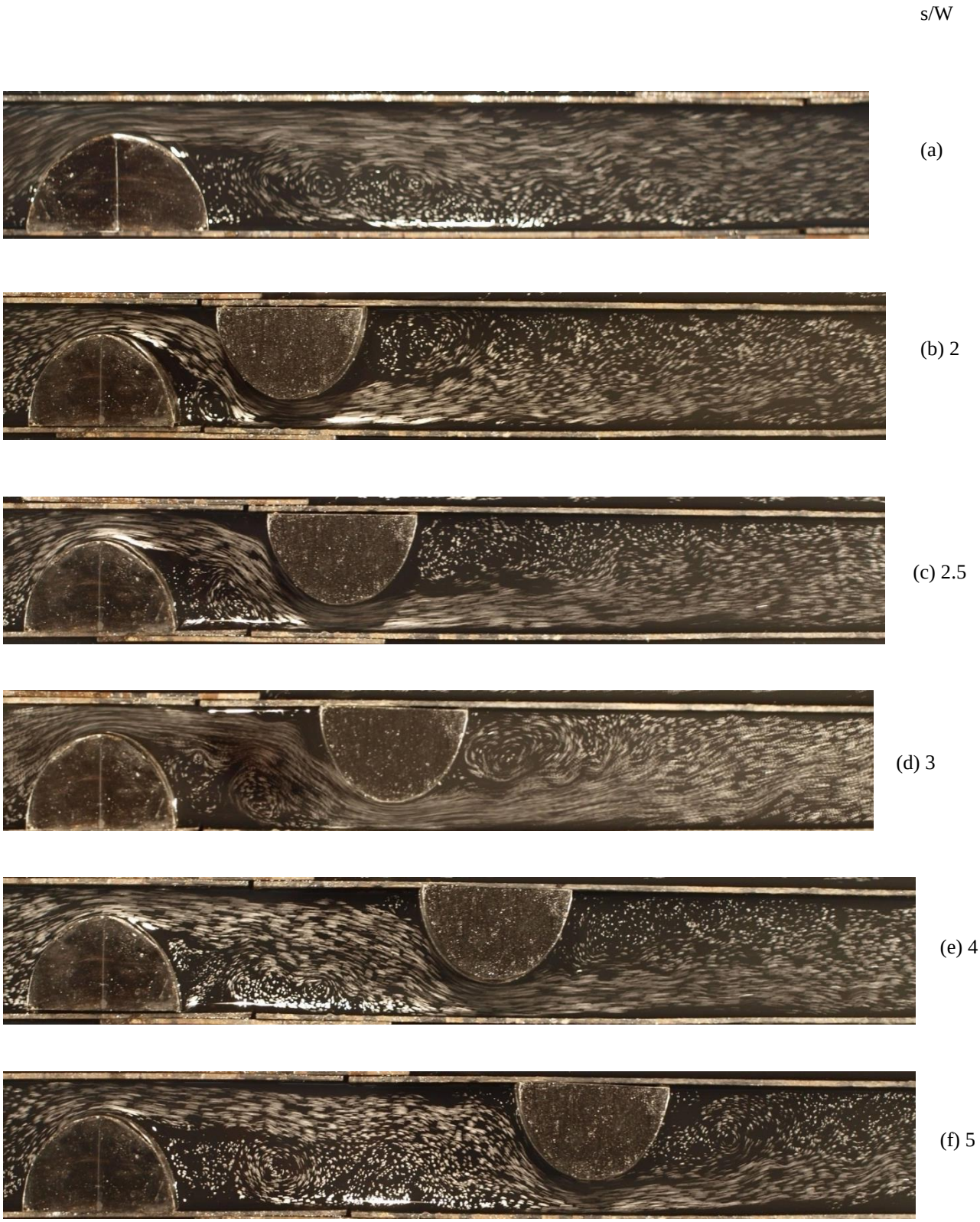

Fig.11 Flow pattern for r/W=0.75, r_i/W=0.75, for various s/W ratio.

(This work is licensed under a Creative Commons Attribution 4.0 International License.)

International Journal of Engineering Research & Technology (IJERT)
ISSN: 2278-0181
Vol. 7 Issue 02, February-2018

s/W

(a)

(b) 2

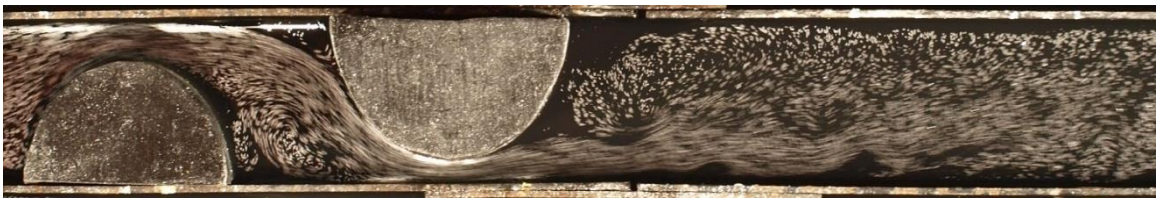

(c) 2.5

(d) 3

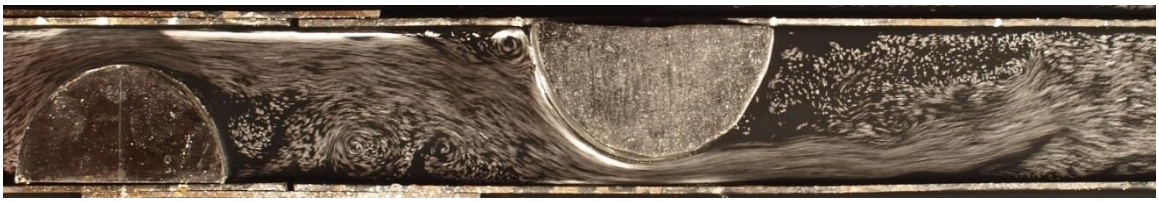

(e) 4

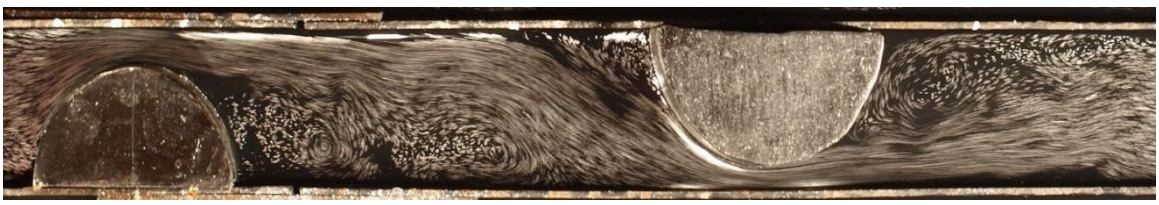

(f) 5

Fig.12 Flow pattern for r/W=0.75, r_i/W=0.9, for various s/W ratio.

(This work is licensed under a Creative Commons Attribution 4.0 International License.)

International Journal of Engineering Research & Technology (IJERT)
ISSN: 2278-0181
Vol. 7 Issue 02, February-2018

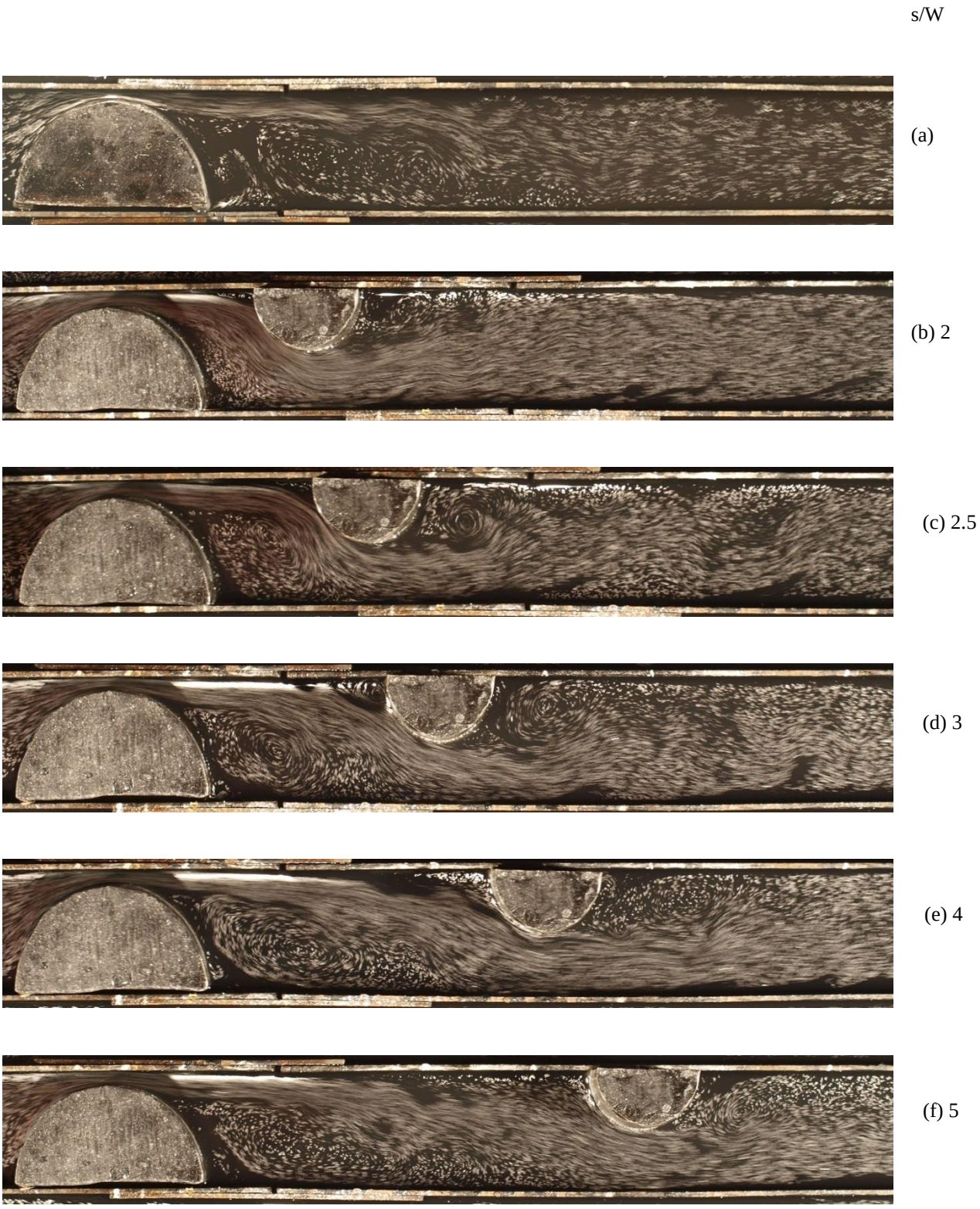

Fig.13 Flow pattern for r/W=0.9, r_i/W=0.5, for various s/W ratio.

(This work is licensed under a Creative Commons Attribution 4.0 International License.)

International Journal of Engineering Research & Technology (IJERT)
ISSN: 2278-0181
Vol. 7 Issue 02, February-2018

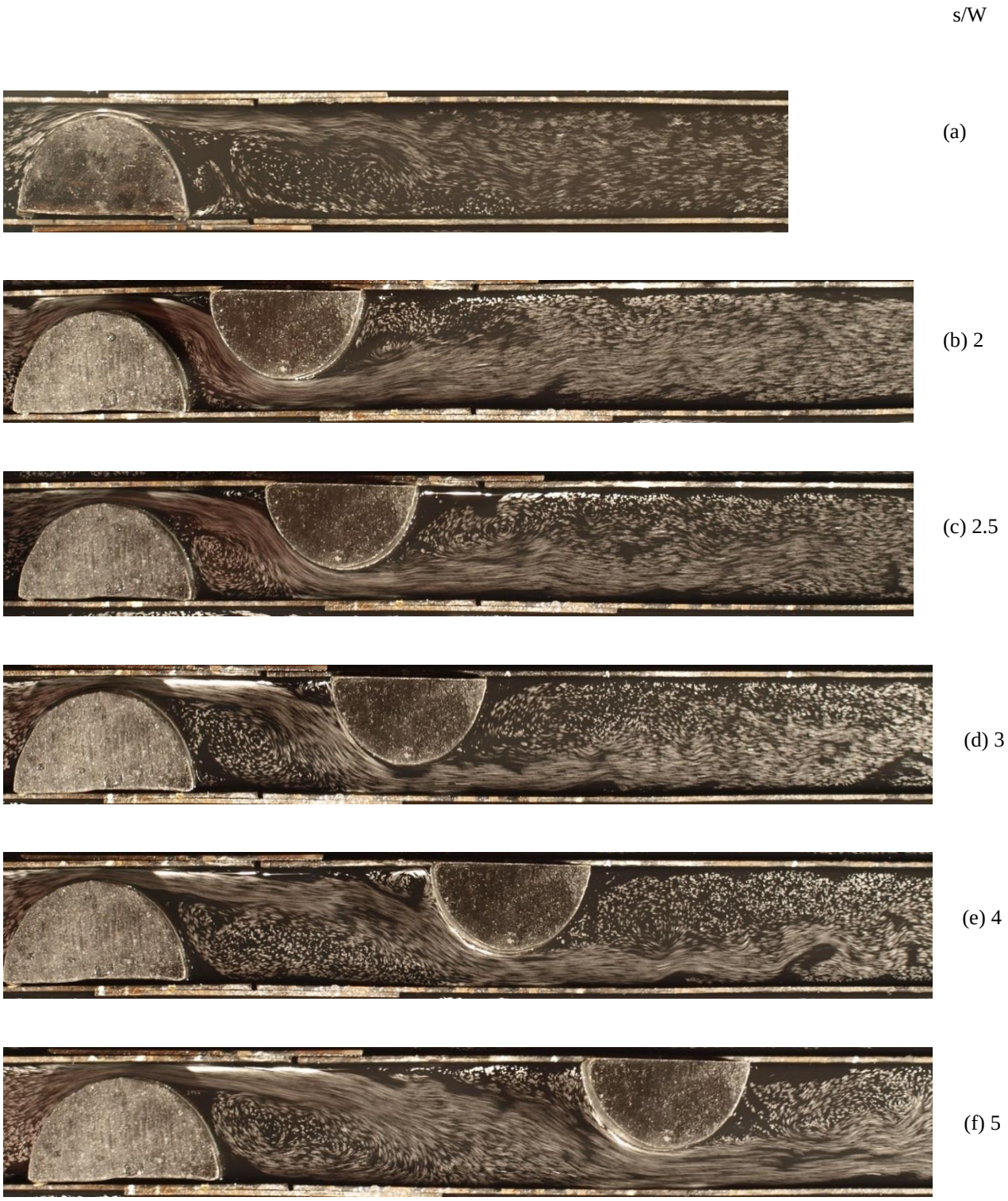

Fig.14 Flow pattern for r/W=0.9, r_i/W=0.75, for various s/W ratio.

(This work is licensed under a Creative Commons Attribution 4.0 International License.)

International Journal of Engineering Research & Technology (IJERT)
ISSN: 2278-0181
Vol. 7 Issue 02, February-2018

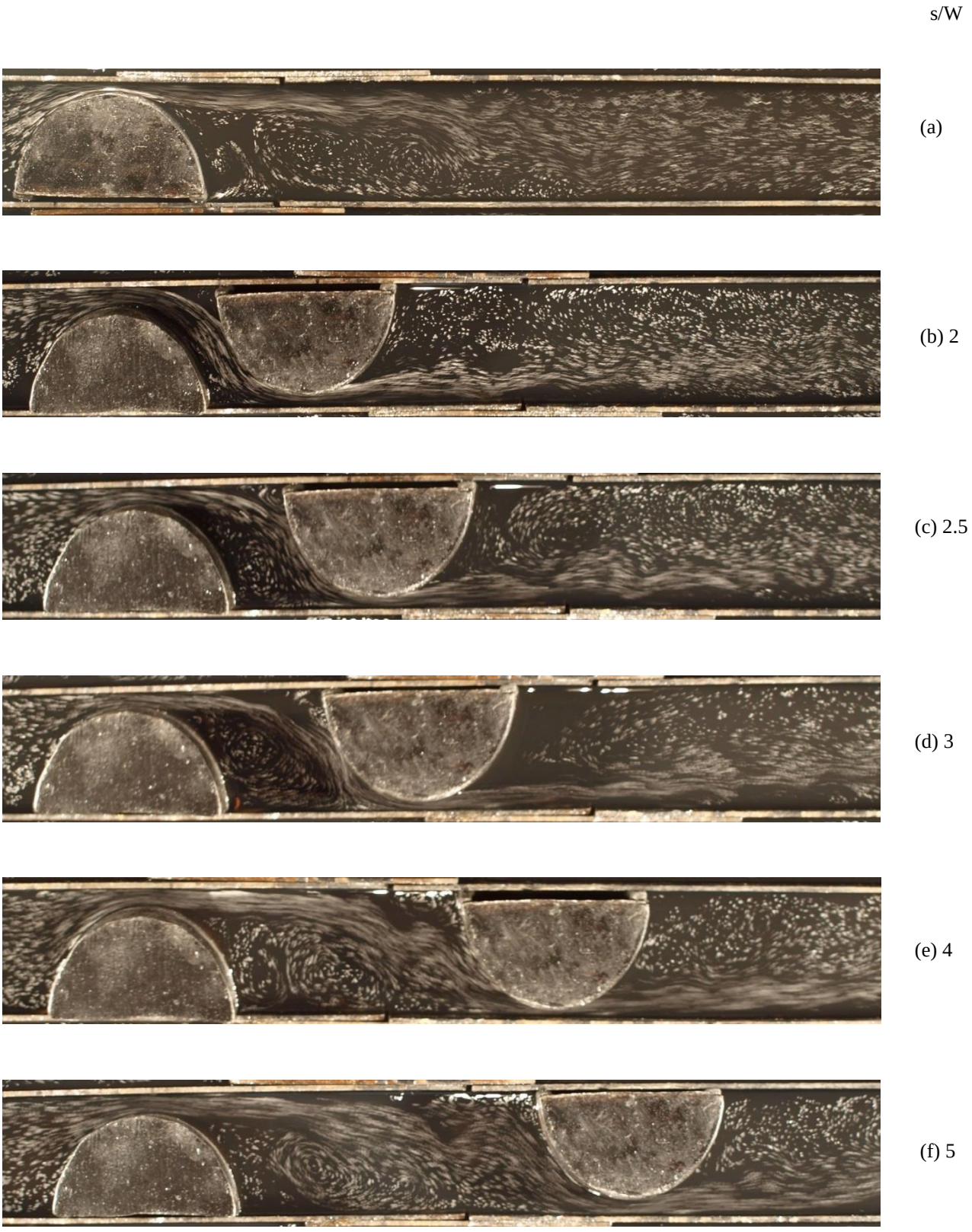

Fig 15: Flow pattern for r/W=0.9, r_i/W=0.9, for various s/W ratio.

(This work is licensed under a Creative Commons Attribution 4.0 International License.)